

LETTER • OPEN ACCESS

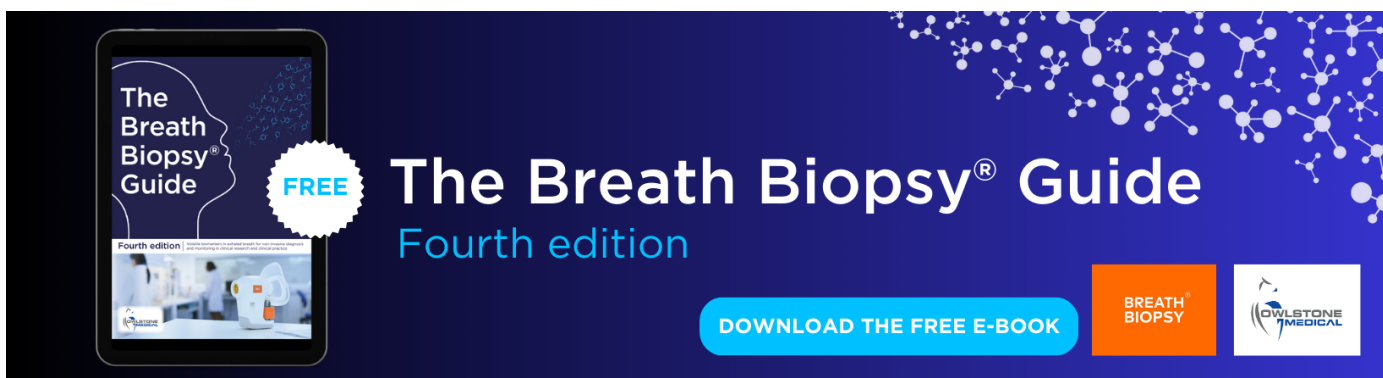
Fragmented tipping in a spatially heterogeneous world

To cite this article: Robbin Bastiaansen *et al* 2022 *Environ. Res. Lett.* **17** 045006

View the [article online](#) for updates and enhancements.

You may also like

- [Climate change induced socio-economic tipping points: review and stakeholder consultation for policy relevant research](#)
Kees C H van Ginkel, W J Wouter Botzen, Marjolijn Haasnoot *et al*.
- [Estimating rate-induced tipping via asymptotic series and a Melnikov-like method](#)
Christian Kuehn and Iacopo P Longo
- [Perspectives on tipping points in integrated models of the natural and human Earth system: cascading effects and telecoupling](#)
Christian L E Franzke, Alessio Ciullo, Elisabeth A Gilmore *et al*.



The Breath Biopsy® Guide
Fourth edition

FREE

DOWNLOAD THE FREE E-BOOK

BREATH BIOPSY

OWLSTONE MEDICAL

ENVIRONMENTAL RESEARCH
LETTERS

LETTER

Fragmented tipping in a spatially heterogeneous world

Robbin Bastiaansen^{1,*} , Henk A Dijkstra^{1,2} and Anna S von der Heydt^{1,2} ¹ Department of Physics, Institute for Marine and Atmospheric Research Utrecht, Utrecht University, Utrecht, The Netherlands² Department of Physics, Centre for Complex System Studies, Utrecht University, Utrecht, The Netherlands

* Author to whom any correspondence should be addressed.

E-mail: r.bastiaansen@uu.nl**Keywords:** tipping points, spatial heterogeneity, pattern formation, climate resilience, climate change

OPEN ACCESS

RECEIVED

30 November 2021

REVISED

18 February 2022

ACCEPTED FOR PUBLICATION

1 March 2022

PUBLISHED

14 March 2022

Original Content from this work may be used under the terms of the [Creative Commons Attribution 4.0 licence](https://creativecommons.org/licenses/by/4.0/).

Any further distribution of this work must maintain attribution to the author(s) and the title of the work, journal citation and DOI.

**Abstract**

Many climate subsystems are thought to be susceptible to tipping—and some might be close to a tipping point. The general belief and intuition, based on simple conceptual models of tipping elements, is that tipping leads to reorganization of the full (sub)system. Here, we explore tipping in conceptual, but spatially extended and spatially heterogeneous models. These are extensions of conceptual models taken from all sorts of climate system components on multiple spatial scales. By analysis of the bifurcation structure of such systems, special stable equilibrium states are revealed: coexistence states with part of the spatial domain in one state, and part in another, with a spatial interface between these regions. These coexistence states critically depend on the size and the spatial heterogeneity of the (sub)system. In particular, in these systems the crossing of a tipping point not necessarily leads to a full reorganization of the system. Instead, it might lead to a reorganization of only part of the spatial domain, limiting the impact of these events on the system's functioning.

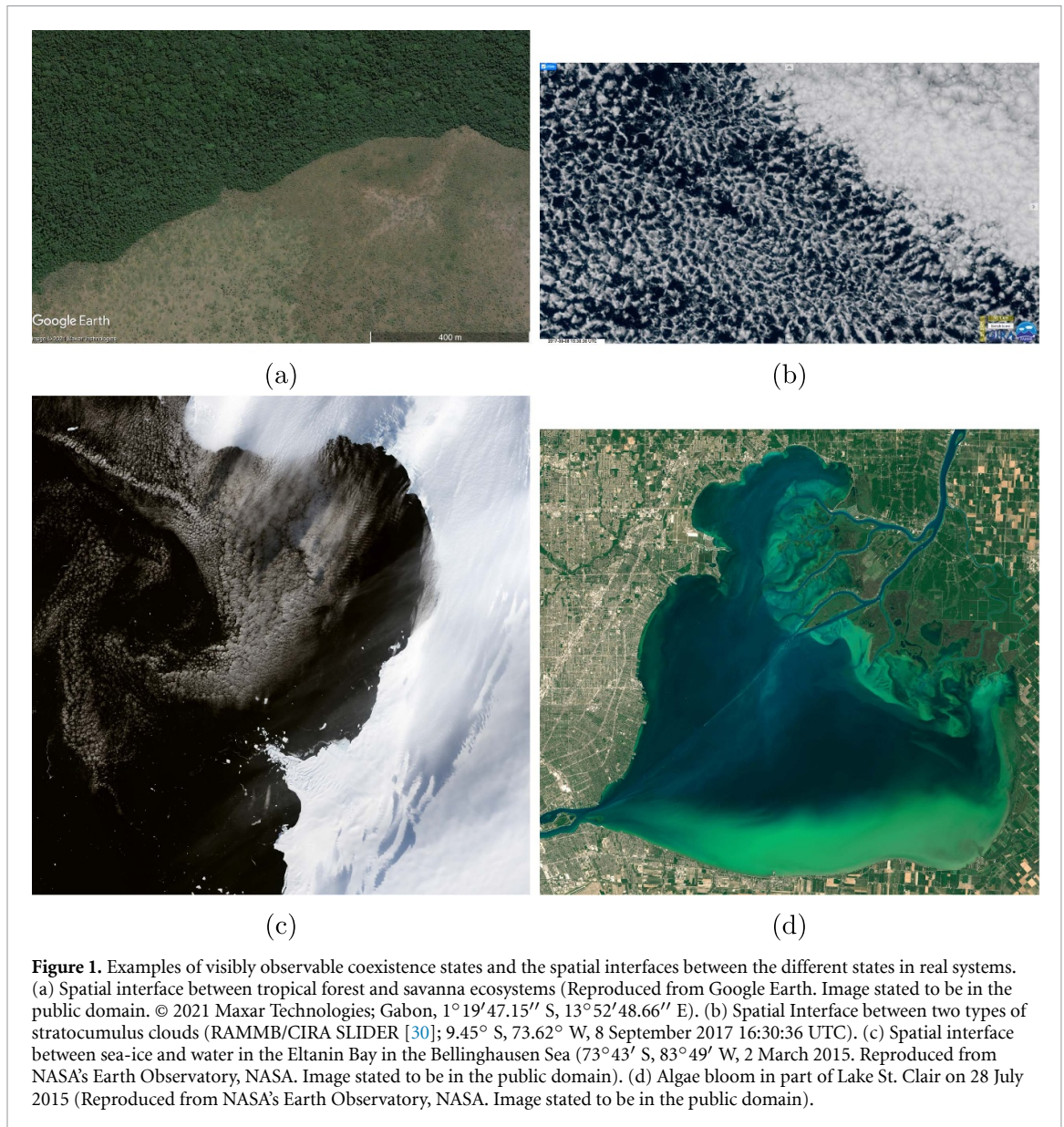
1. Introduction

Many Earth system components and ecosystems have been shown to exhibit tipping [1–5]: when a tiny change in environmental conditions or parameters leads to a critical shift towards an alternative state that might have completely different functioning. For instance, the Amazonian rainforest that might disappear [6, 7], desertification [8, 9], a restructuring of the Atlantic meridional overturning circulation [10, 11], collapses of ice sheets [12–14], turbidity in shallow lakes [15], amongst many others. Even on a planetary scale, tipping might have happened [16], and is hypothesised to be possible in the (near) future [17–19].

Typically, tipping is illustrated and explained using simple, conceptual low-dimensional models, that have two alternative states and that can tip between them as climatic conditions change [1–3, 20]. In more complex, more detailed high-dimensional models and in real-life data tipping is, however, often not as clear and pronounced [4, 5, 21]. Tipping from one state to a completely differently structured state is hardly ever observed. Instead, partial restructurings occur more often. For instance, (large) parts of an ice sheet melt, instead of the whole sheet melting in one single tipping event [22].

This suggests that low- and high-dimensional models behave differently. It could be that high-dimensional models are tuned for stability too much, suppressing tipping behaviour [23]. It could also be that the low-dimensional models are too restrictive in the number of physical processes, thereby exaggerating tipping behaviour [24, 25]. At least, the most simple models really only allow for two alternative states and nothing more. Adding complexity to these leads to more response options for the system, which might lead to less severe tipping events. For instance, adding more boxes to a box model [26, 27], or incorporating spatial effects [21, 25].

In this paper, we investigate the behaviour of conceptual models when spatial effects are incorporated: spatial transport and spatial heterogeneity. This setting has received only little attention in the literature [21, 28] and a thorough theoretical understanding of such systems is still lacking, despite their omnipresence [29]. In such models additional stable states called *co-existence states* can emerge, in which part of the domain resides in one state and the rest in another state, with a spatial interface separating these regions [21, 24]—see figure 1 for real-life examples. Consequently, in these systems transitions can occur in which only in part of the spatial domain the system



changes state, providing a more subtle, fragmented tipping pathway.

The rest of this paper is structured as follows. In section 2, we first review the classic theory of coexistence states in spatially homogeneous (gradient) systems. Subsequently, we detail how this theory changes in a spatially heterogeneous setting. We focus on the possibility of new equilibrium coexistence states and the different bifurcation diagrams these systems can have depending on the spatial heterogeneity. Then, in section 3, we illustrate the potential widespread relevance of coexistence states using several examples of climate subsystems on different spatial scales. For this, we use a variety of conceptual models, that have been proposed before in the literature, or spatially extended versions thereof. Finally, we end with a discussion in section 4.

2. Theory

We consider the evolution of a (single) state variable y . Depending on the particular system of interest, this could be for example temperature or vegetation coverage. Ignoring spatial effects for a moment, the local dynamics of y are described by an ordinary differential equation, i.e.

$$\frac{dy}{dt} = f(y; \mu) =: \frac{\partial V}{\partial y}(y; \mu), \quad (1)$$

where f describes the evolution over time, depending on the value of the state variable y and the value of a (bifurcation) parameter μ , and V is the associated potential function (also referred to as the stability landscape) [1–3].

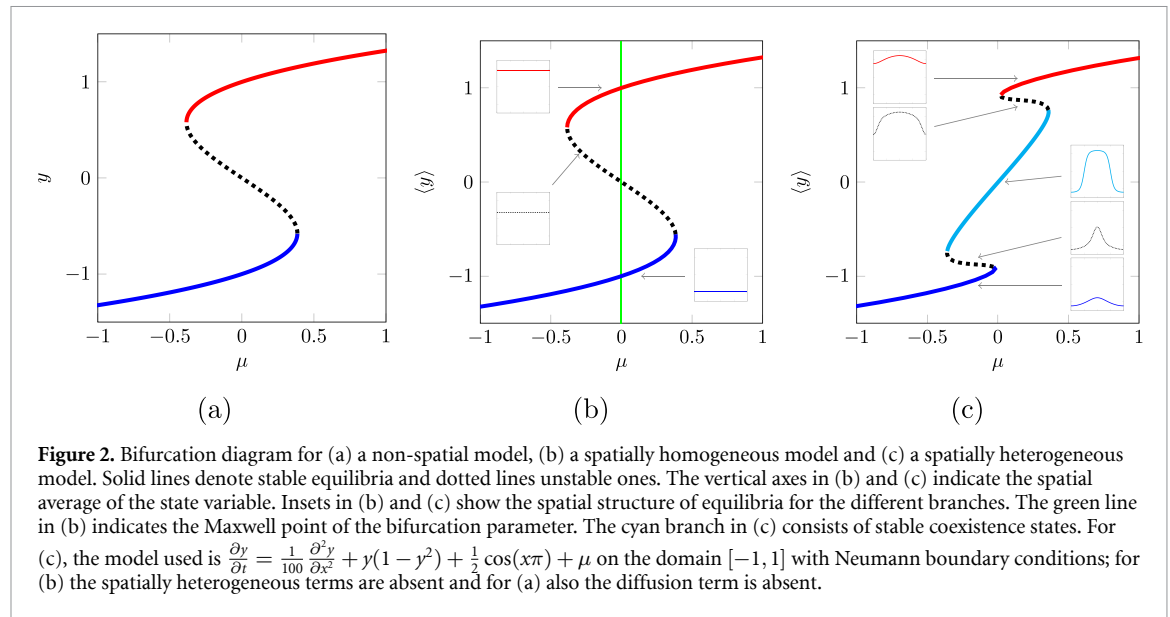


Figure 2. Bifurcation diagram for (a) a non-spatial model, (b) a spatially homogeneous model and (c) a spatially heterogeneous model. Solid lines denote stable equilibria and dotted lines unstable ones. The vertical axes in (b) and (c) indicate the spatial average of the state variable. Insets in (b) and (c) show the spatial structure of equilibria for the different branches. The green line in (b) indicates the Maxwell point of the bifurcation parameter. The cyan branch in (c) consists of stable coexistence states. For (c), the model used is $\frac{\partial y}{\partial t} = \frac{1}{100} \frac{\partial^2 y}{\partial x^2} + y(1 - y^2) + \frac{1}{2} \cos(x\pi) + \mu$ on the domain $[-1, 1]$ with Neumann boundary conditions; for (b) the spatially heterogeneous terms are absent and for (a) also the diffusion term is absent.

The model (1) possesses tipping behaviour when there is a parameter region in which there is bistability of two different states—say, a state *A* and state *B*—with tipping points (saddle-node bifurcations) to the other state at both ends of this region. This leads to the prototypical ‘S’-curve bifurcation diagram as shown in figure 2(a). An explicit example of such system is the model (1) with

$$V(y; \mu) = \frac{y^2}{2} - \frac{y^4}{4} + \mu y. \quad (2)$$

In the rest of this section, we detail how the addition of spatial effects to the model (1) changes the bifurcation diagram.

2.1. Spatial transport

We now consider the evolution of the state variable *y* on a spatial domain with coordinate *x*. In addition to the local dynamics, spatial transport between locations now also plays a role. The most simple way to implement spatial transport is to add (linear) diffusion to the model (1). Thus, a new spatial model describing the evolution of *y* over time and space is given by the partial differential equation

$$\frac{\partial y}{\partial t} = D\Delta y + f(y; \mu) = D\Delta y + \frac{\partial V}{\partial y}(y; \mu), \quad (3)$$

where *D* is the diffusion coefficient and Δ the spatial Laplacian in *x*.

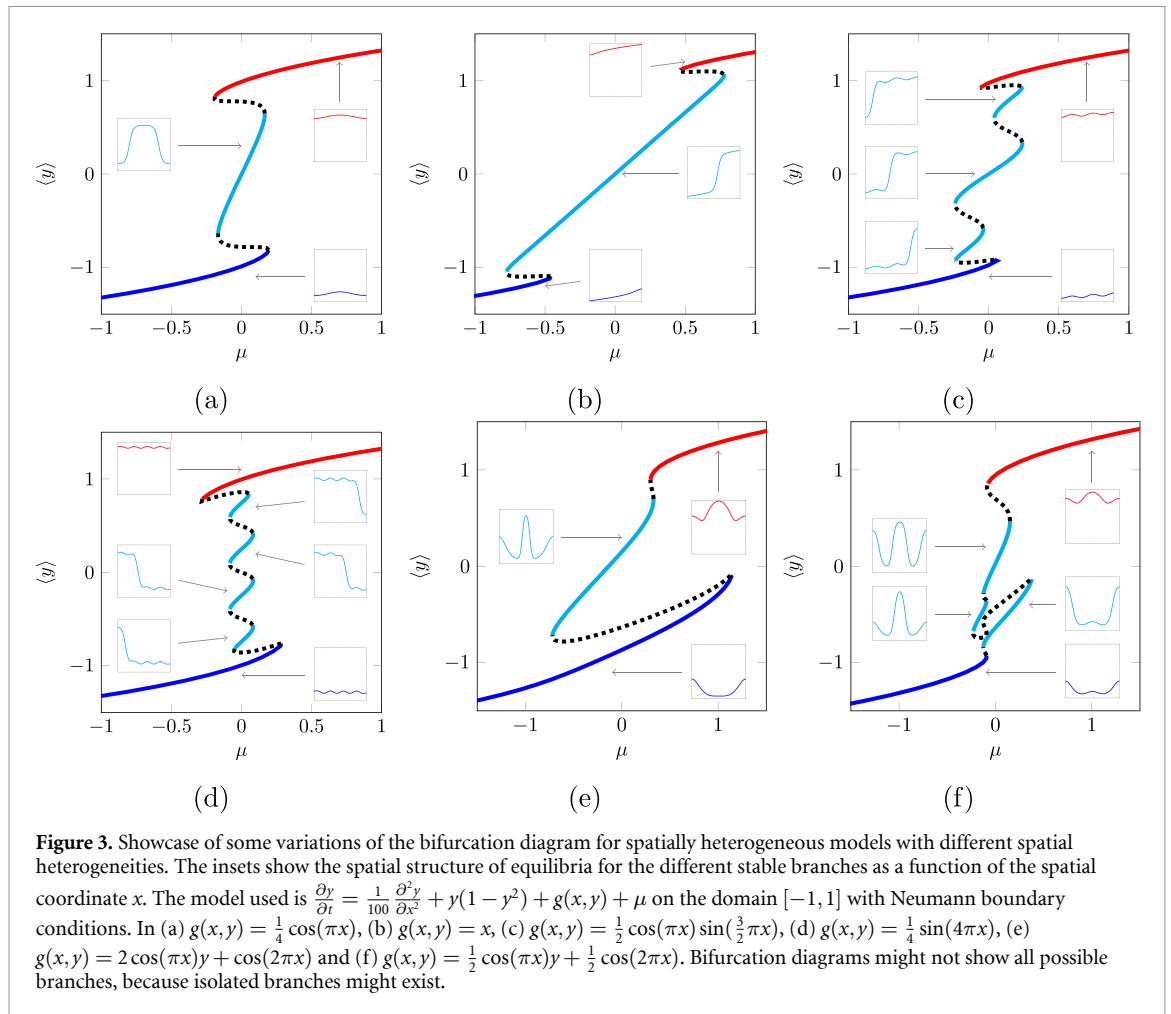
Because this type of model can be used to model phase segregation dynamics [31, 32], its dynamics are well understood and the literature is quite extensive, including rigorous mathematical proofs [33, 34]. First, spatially uniform states exist in which the whole domain is in the same state (either state *A* or *B*). These are the natural spatially extended versions of the states in the local model (1). However, next to these, there

are also coexistence states, in which parts of space reside in state *A* and the rest in state *B*, with a spatial interface (or ‘front’ in mathematical jargon) connecting these regions. These interfaces can be spatially localized, or extend over a large space depending on the strength of the spatial transport.

The dynamics of these coexistence states is intricate [33, 35]. In short: the interfaces typically migrate slowly over space depending on the distance to other interfaces and the domain boundary, but there are sometimes fast coalescence events when interfaces meet and separate regions merge. On the long term, a maximum of one interface can persist in the domain (the rest is slow transient behaviour). Such single interface moves with a speed that is proportional to the difference in potential between states *A* and *B*, i.e. $V(A; \mu) - V(B; \mu)$. So, only in the degenerate case in which the potentials are equal, this leads to an additional equilibrium state of (3). The specific parameter value for which the potentials are equal is called the *Maxwell point* of the system. This means that the bifurcation diagram does not change much compared to the non-spatial system; see figure 2(b). However, the transient dynamics occurring after a tipping point has been crossed can be different in such systems: this can now occur via an invasion front which replaces one state with the other, which might lead to a slow tipping of the full system [36, 37].

2.2. Spatial heterogeneity

The previous model (3) assumes that the local dynamics are the same throughout the whole domain, i.e. the model is spatially homogeneous. Reality is, however, spatially heterogeneous: local dynamics differ from location to location, for example due to topographical features or human activity. Hence, it is more realistic to consider a spatially extended model in



which the local dynamics explicitly depends on the location x :

$$\frac{\partial y}{\partial t} = D\Delta y + f(y, x; \mu) = D\Delta y + \frac{\partial V}{\partial y}(y, x; \mu). \quad (4)$$

We will assume that the spatial variation is not too much locally, i.e. $\frac{\partial f}{\partial x}(y, x; \mu)$ does not get very large compared to diffusion strength (as this would, potentially, give rise to different dynamics than described in this paper; see e.g. [38, 39] for an exploration of those dynamics in case of spatially periodic forcings).

The presence of spatial heterogeneity in (4) does change the dynamics of the interfaces. Their movement now depends on the *local* difference between the potentials of state A and B . Because of this, the Maxwell point is different for different locations in space, making it no longer a degenerate case. Furthermore, coexistence states with multiple interfaces can now be equilibrium states of the model system.

A typical bifurcation diagram is given in figure 2(c), which is different compared to the classic one (figure 2(a)) because of the additional branch of stable coexistence states. In this case, the crossing of a tipping point does not necessarily lead to a tipping of the complete system, but can lead to a less critical shift

of the system in which only part of the spatial domain undergoes a transition to the alternative state.

The precise structure of the bifurcation diagram depends on the specific heterogeneity of the system. A few possible variations are shown in figure 3, illustrating the potential complexity of the bifurcation diagram for spatially heterogeneous systems. The results show that the parameter range for which coexistence states exist can vary much between systems with different heterogeneities. In particular, this range can be fully contained in the hysteresis loop of the non-coexistence states (e.g. (a) and (d)), which indicates that crossings of the tipping points will lead to a full tipping of the system despite the presence of coexistence states in part of the parameter regime. On the other hand, the spatial heterogeneity can also prevent overlap of the fully tipped branches (e.g. (b)), meaning that the full system cannot tip in one tipping event. It can also happen that the tipping process is fragmented in one direction, but not in other directions (e). Moreover, the spatial heterogeneity can lead to multiple tipping points (e.g. (c), (d) and (f)), in each of which another part of the spatial domain undergoes a transition to the alternative state.

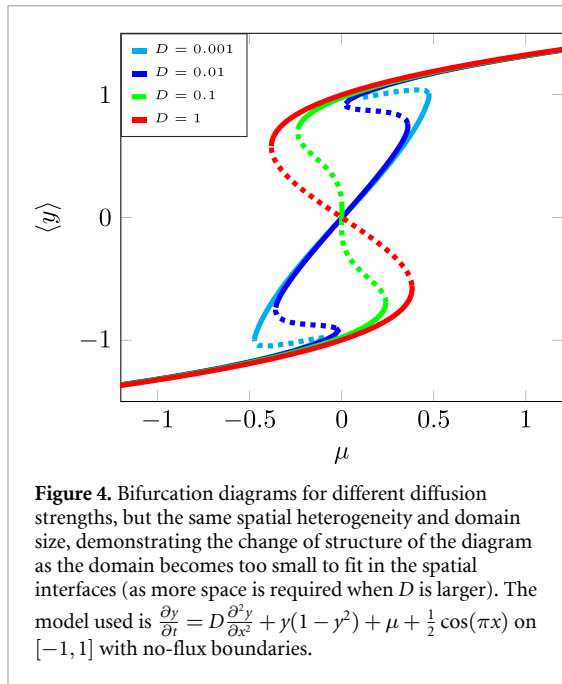


Figure 4. Bifurcation diagrams for different diffusion strengths, but the same spatial heterogeneity and domain size, demonstrating the change of structure of the diagram as the domain becomes too small to fit in the spatial interfaces (as more space is required when D is larger). The model used is $\frac{\partial y}{\partial t} = D \frac{\partial^2 y}{\partial x^2} + y(1 - y^2) + \mu + \frac{1}{2} \cos(\pi x)$ on $[-1, 1]$ with no-flux boundaries.

A concise description of the mathematical theory and analysis of coexistence states can be found in appendix A.

The above described spatial interfaces between regions in different states can only emerge and persist if there is enough space available for them in the system. Hence, if the spatial domain is too confined, the above described coexistence states do not fit and the branch of coexistence states is absent in the bifurcation diagram (see figure 4). The precise minimum required length varies per model and depends on the typical length scale associated with the spatial transport. For instance, if the diffusion coefficient D in (4) is increased, a larger domain is needed to facilitate the coexistence states. See also appendix B for a mathematical treatment of the small domain limit.

The form of equation (4) is chosen for simplicity of presentation. Coexistence states can also occur in other models that for example have a diffusion coefficient that depends on space or have a different spatial transport mechanism altogether. Similar behaviour as described above can at least be expected from other spatially heterogeneous Lagrangian or gradient systems.

3. Earth system and ecosystem example conceptual models

The above described theory is quite generic, and there are only few assumptions. Hence, if a simple conceptual model only considers local dynamics and captures tipping behaviour, a spatially extended and heterogeneous model will behave as described above. In particular, such systems might have additional coexistence states, and tipping events in which only part of the domain undergoes transition. Many systems, and many previously proposed conceptual models,

fit into this description. To illustrate this, next we give some examples of systems for which this theory might be relevant by looking at some illustrative conceptual spatially extended models for these systems. These are either models directly taken from the literature or simple spatial extensions of non-spatial models. Hereby we cover systems of many different spatial scales, ranging from global to more regional systems.

3.1. Global energy balance model

On a planetary scale, an example of coexistence states can be found in global energy balance models. These describe the evolution of Earth's temperature by considering the energy flux at the top of the atmosphere. These type of models were first introduced by Budyko [40] and Sellers [41], and have since served often as conceptual models to illustrate planetary climate shifts [42–52].

Here, we consider the following simple spatially one-dimensional variant:

$$C_T \frac{\partial T}{\partial t} = Q_0(x) [1 - \alpha(T)] - \varepsilon \sigma_0 T^4 + \mu + D \frac{\partial}{\partial x} \left[(1 - x^2) \frac{\partial T}{\partial x} \right]. \quad (5)$$

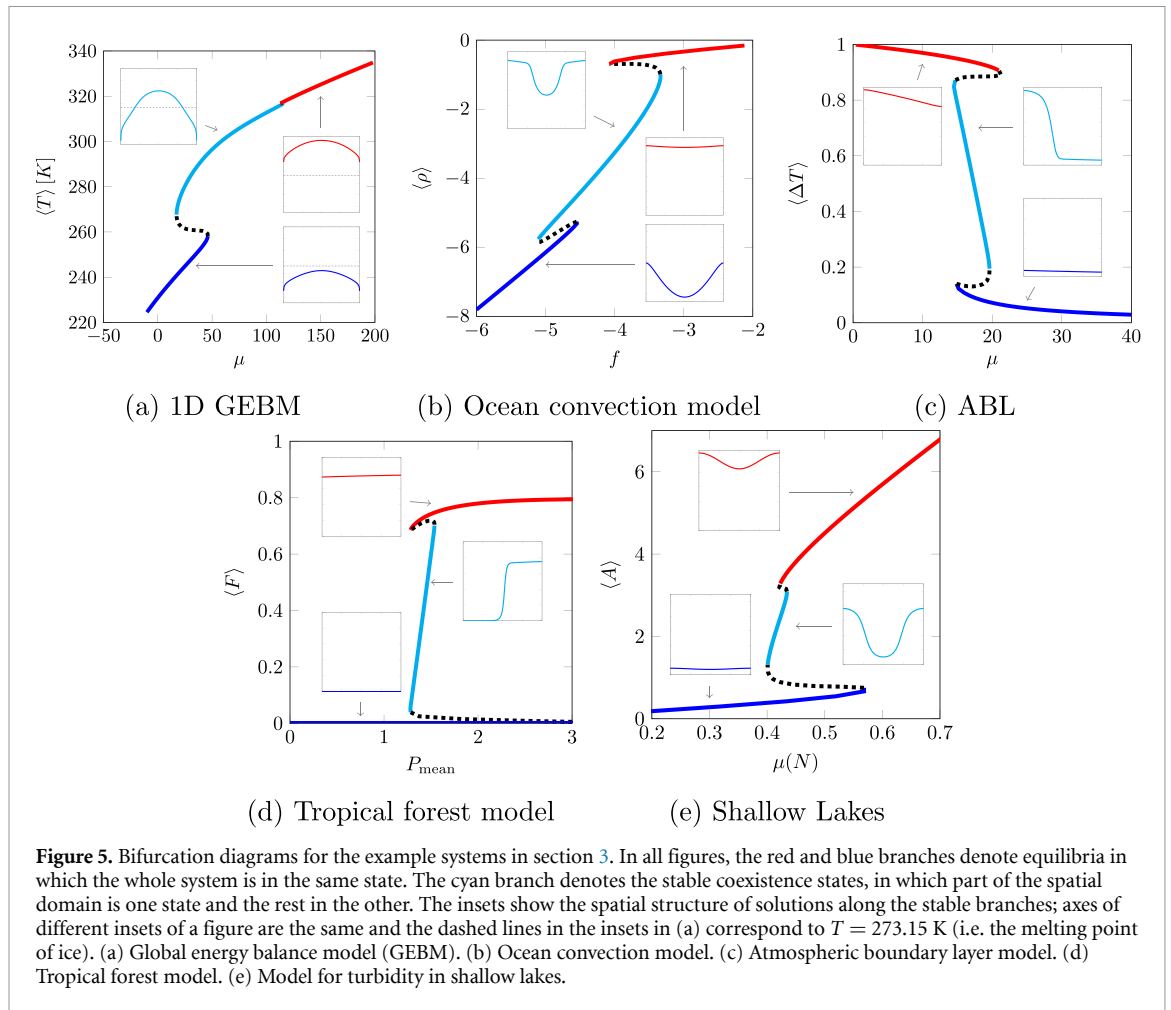
This models the longitudinally averaged temperature T (as function of $x = \sin(\theta)$ where θ is the latitude) by looking at the absorbed incoming solar radiation ($Q_0(x) [1 - \alpha(T)]$), the outgoing Planck radiation ($-\varepsilon \sigma_0 T^4$), the meridional heat transport ($+D \frac{\partial}{\partial x} [(1 - x^2) \frac{\partial T}{\partial x}]$), and the effect of atmospheric CO_2 on the energy budget ($+\mu$). The model uses the following functional form for the temperature-dependent albedo (ice, with a high albedo, can only exist if temperatures are low enough):

$$\alpha(T) = \alpha_1 + (\alpha_2 - \alpha_1) \frac{1 + \tanh\left(M \left[T - \frac{T_1 + T_2}{2}\right]\right)}{2}, \quad (6)$$

where α_1 is the albedo of ice, and α_2 the albedo of water. The sigmoid function ensures the change in albedo is smooth. The spatial heterogeneity in this models stems from the incoming solar radiation, which is latitude-dependent. Following [48], we have taken

$$Q(x) = Q_0 (1 - 0.241 [3x^2 - 1]), \quad (7)$$

where Q_0 is the global average of the incoming solar radiation. As parameters we have taken $Q_0 = 341.3 \text{ W m}^{-2}$, $\alpha_1 = 0.289$, $\alpha_2 = 0.70$, $T_1 = 260 \text{ K}$, $T_2 = 290 \text{ K}$, $M = 0.1 \text{ K}^{-1}$, $\varepsilon = 0.61$, $\sigma_0 = 5.67 \times 10^{-8} \text{ W m}^{-2} \text{ K}^{-1}$. The value for the diffusivity D is not known—and potentially not uniform over earth [44, 45]—but for the illustrative purposes in this paper we have taken $D = 0.30$. Finally, since we are focussing on stationary states, the value for



C_T does not matter, but a typical value would be $C_T = 5 \times 10^8 \text{ J m}^{-2} \text{ K}^{-1}$.

It has been shown that the model can reside in an ice-free state or a fully ice-covered ‘Snowball Earth’ state. When spatial effects are not modelled, these are the only states of the model. However, once spatial effects are incorporated, planet-scale coexistence states are also found with ice in only part of the earth (i.e. the poles) and no ice elsewhere [42–51]. An example bifurcation diagram is given in figure 5(a) which shows the global mean temperature as function of the parameter μ . This diagram shows that tipping between a snowball earth state (blue branch) and a partially ice covered state (cyan branch) leads to large changes in global temperature, whereas tipping between coexistence states (cyan branch) and ice-free states (red branch) leads to much smaller changes in global temperature. It is also interesting to note that there is no bistability of snowball earth and ice-free states, implying that transitions between them always need to go via coexistence states.

3.2. Ocean circulation

In oceans, convection occurs at places where the ocean mixed-layer exchanges water with the deep ocean. This ocean convection plays an important role

in the global ocean circulation. Using simple conceptual models, the possibility of bistability between a convective and a non-convective state has been found for a range of parameters [53–56]. These results have been obtained in box models, where temperature T and salinity S of the mixed-layer are dynamic variables, which change through exchange with (static) atmosphere and deep ocean boxes. Here, we extend such model via the addition of diffusion as form of spatial transport.

To showcase coexistence states with convection only at certain regions, we apply a series of (standard) simplifications on the equations (details in appendix C). This leads to the following equation that describes the evolution of the local density difference $\Delta\rho(x, t)$ between the mixed-layer and the deep ocean:

$$\frac{\partial \Delta\rho}{\partial t} = D \frac{\partial^2 \Delta\rho}{\partial x^2} + k_T (\Delta\rho_A(x) - \Delta\rho) - \kappa(\Delta\rho)\Delta\rho + D \frac{\partial^2 \rho_0(x)}{\partial x^2}. \quad (8)$$

Here, $\Delta\rho_A(x)$ represents the (static) density difference between the atmosphere box and the deep ocean box, and $\rho_0(x)$ is the local density in the deep ocean box. Further, k_T gives the rate of exchange with the atmosphere box and $\kappa(\Delta\rho)$ the rate of exchange with

the deep ocean box. The latter is a function of $\Delta\rho$, which is a non-negative increasing function [53]. That is, convection happens when the exchange rate $\kappa(\Delta\rho)$ is large, which typically occurs if the mixed-layer is heavy enough compared to the deep ocean.

Depending on the functional form of the exchange rate $\kappa(\Delta\rho)$, certain parameter ranges can allow for bistability and coexistence states between convection and no convection. Not striving for the most realistic description, we take a continuous approximation of a step function similar to [53]. Specifically, we take $\kappa(\Delta\rho) = \frac{\bar{\kappa}}{2} [1 + \tanh(\Delta\rho - \Delta\rho_{\text{ref}})]$ which goes from 0 to $\bar{\kappa}$ and starts to increase around $\Delta\rho_{\text{ref}}$. As parameter values we have taken $k_T = 1$, $\bar{\kappa} = 100$, $\Delta\rho_{\text{ref}} = -1/2$ and $\rho_0(x) \equiv 0$. In the numerical computations we have rescaled the spatial domain to $[-1, 1]$ and have taken $D = 0.01$. As the horizontal diffusion coefficient of ocean systems is typically between 100 and 1000 $\text{m}^2 \text{s}^{-1}$ this corresponds to an ocean basin of about 100–1000 km in size.

To illustrate this model, we take a spatially heterogeneous atmospheric reference density $\Delta\rho_A(x) = 2 + f(1 + \cos[\frac{\pi x}{2}])$, where f acts as a bifurcation parameter. In ocean systems, such kind of spatial heterogeneity could for instance be caused by local differences in freshwater fluxes. In figure 5(b), an example bifurcation diagram for this model is given, showing the possibility of coexistence states in large enough ocean basins. In this system, the system does not tip fully between convective and non-convective states at a tipping point, but only part of the domain changes and the system transitions to a coexistence state—for chosen heterogeneity, in these coexistence states convection happens only at the edges of the spatial domain.

3.3. Atmospheric circulation

In the atmospheric circulation, there also seems to be the possibility of coexistence states. As a simple example, we look at the dynamics of the atmospheric boundary layer, in which heat exchange with the surface takes place. This boundary layer can be in a fully turbulent state or a quiescent, quasi-laminar state depending on the temperature difference between the boundary layer and the soil. In cold regions, or during cold nights, the layer is stable stratified, but at higher temperatures surface warming leads to a convective boundary layer.

Bistability and tipping between these two states has been explained using simple energy balance models [57, 58]. These describe the near-surface inversion strength ΔT , defined roughly as the boundary layer's temperature minus the soil temperature, which evolves according to the net imbalance of the energy fluxes in the layer [58]. To the best of our knowledge, there is no standard way to include spatial heat redistribution. Hence, as a first effort to create a spatially extended model, we have modelled spatial heat

re-distribution as a diffusive process. The model is given by

$$\frac{\partial \Delta T}{\partial t} = D \frac{\partial^2 \Delta T}{\partial x^2} + Q(x) - \lambda \Delta T - C(x) \Delta T e^{-2\alpha \Delta T}. \quad (9)$$

Here, $Q(x) - \lambda \Delta T$ is the linearized net long-wave radiation, and $-C(x) \Delta T e^{-2\alpha(\Delta T)}$ is the turbulent sensible heat flux. The location x can be interpreted as a local coordinate of a larger region on Earth. In the numerical computations, we have rescaled the spatial domain to $[-1, 1]$ and have taken a rescaled diffusion coefficient $D = 0.01$. In reality, this would correspond to a spatial domain that is much larger than the diffusion length scale.

To demonstrate the effect of spatial heterogeneity in this model, we take $\lambda = 1$, $\alpha = 3$, $Q(x) = 1 - 0.1x$ and $C(x) = 0.1x + \mu$, modelling for example spatial differences in soil temperature or wind speeds (the latter influences the turbulent sensible heat flux); μ acts here as a bifurcation parameter, representing changes in wind speed. For these choices, an example bifurcation diagram is given in figure 5(c), which indicates the possibility of coexistence states with regional turbulence. However, for these heterogeneous conditions, the branch of coexistence states is almost fully contained in the hysteresis loop of the fully turbulent and the fully quasi-laminar states, suggesting that crossings of the tipping points might lead to a full tipping of the system despite the presence of a branch of coexistence states in the bifurcation diagram.

3.4. Ecosystems

In many ecological systems, bistability and transitions between alternative states have been found. For instance, in drylands, bistability between vegetation and bare soil occurs [59]. On larger scales, the same environmental conditions can even support multiple ecosystem types, such as grasslands, savannas and tropical forests in the Tropics [7, 60]. In all of these systems, spatial effects are present: species disperse over space (e.g. via seed dispersal) and environmental conditions are spatially heterogeneous (e.g. a rainfall gradient). Hence, they can exhibit coexistence states in which different ecosystem types are separated by a local interface.

Especially in models of drylands, many patterned states have been analyzed, including coexistence states [37, 61], although spatial heterogeneities are not often taken into account, with few exceptions [62, 63]. However, the models considered are typically more complicated than (4) and more advanced mathematical techniques are used to analyze them that are beyond the scope of this article. Hence, we illustrate the coexistence patterns in ecosystems using a different example.

Recently, the bistability between tropical forests and grasslands in a heterogeneous environment has been studied [64]. In a spatially extended (rescaled) version of the model in [65], the local fraction of fire-prone forest trees is given by F and its evolution is modelled as

$$\frac{\partial F}{\partial t} = D \frac{\partial^2 F}{\partial x^2} + r(P)(1-F)F - m(P)F - f(F;P), \quad (10)$$

with the coordinate x representing e.g. a cross-section through a tropical forest region. Here, $r(P) = 0.2(1 - e^{1.54 - 0.003P})$ is the (logistic) growth rate depending on local precipitation $P(x)$. Further, $m(P) = 0.041 + e^{-2.15 - 0.008P}$ is the precipitation-dependent natural mortality rate, and $f(F;P)$ is the mortality due to forest fires, which depends both on the local precipitation $P(x)$ and the local tree coverage F (dry trees burn easier and fire spreads easier when there are less trees and more herbaceous vegetation). Specifically, f takes on the following functional form

$$f(F;P) = \frac{0.46}{2.7} \frac{Y_C(P)^4}{Y_C(P)^4 + f^4}, \quad (11)$$

where $Y_C(P)$ models the assumed decrease in fire-spreading percolation threshold (see [65] for details), expressed in equations as

$$Y_C(P) = \max(0, 0.56 - 1.43 \times 10^{-4}P). \quad (12)$$

Finally, sapling dispersal is modelled as diffusion.

In [64], a 1D spatial domain [0, 3000 km] is taken with diffusivity $D = 0.2$. By rescaling space (see appendix B) this is equivalent to a domain $[-1, 1]$ with $D \approx 5 \times 10^{-6}$. However, we take $D = 10^{-4}$, essentially modelling a smaller real domain of about 100 km.

The spatially heterogeneous term in this example is the local precipitation $P(x)$. Following [64], we have modelled this as a linear precipitation gradient $P(x) = P_{\text{mean}} + 150x$, and model climate change via the mean precipitation parameter P_{mean} . An example bifurcation diagram is given in figure 5(d). Here, the red branch has solutions with non-zero forest tree fraction F everywhere, the blue branch corresponds to a no-forest state and the cyan branch to coexistence states with forest trees in part of the domain. In this diagram, the blue branch is attracting for all parameter values, and does not connect to the other branches via a saddle-node bifurcation (the lower unstable branch only connects to the blue branch in the limit $P_{\text{mean}} \rightarrow \infty$). From the bifurcation diagram it can be deduced that the spatial region with lowest rainfall (left in the insets) will die down when the fully tree-covered state tips into a coexistence state. However, as long as the system is in a coexistence state and there still are trees in part of the domain, restoration is possible if precipitation increases again.

3.5. Shallow lakes

On even smaller spatial scales, coexistence states could also play a role. As an example, we look at the turbidity of shallow lakes [15], which has been used as one of the prime examples of critical shifts in ecological systems. In these lakes, turbidity is closely related to the algae concentration A , which can change depending on the amount of nutrients in the lake. If there is a lot of nutrients, algae concentration is high and the lake is turbid. For lower nutrient concentrations, there are few algae and the lake is clear. Transitions between these states can take place if the nutrient concentration changes.

In [15], a simple non-spatial model is given for the evolution of algae A , depending on the nutrient concentration. Here, we have added spatial transport as a diffusive process to obtain the following spatially explicit model that models the local algae fraction over e.g. a cross-section of a shallow lake:

$$\frac{\partial A}{\partial t} = D \frac{\partial^2 A}{\partial x^2} + r\hat{\mu}(N,x) \frac{A}{1 + V(A,x)} - cA^2; \quad (13)$$

$$V(A,x) = \frac{1}{h_v} \frac{1}{1 + A^{p(x)}}. \quad (14)$$

Here, algae growth is modelled as logistic growth with competition coefficient c . The growth rate depends on the effect of nutrients $\hat{\mu}(N,x)$ and the amount of vegetation $V(A)$, which is larger if there are few algae. The value of $p(x)$ represents the (local) shallowness of the lake. More information on the rescaling process can be found in appendix D.

To illustrate the effect of spatial heterogeneity in such lake systems, we take $\hat{\mu}(x) = \mu(1 - 0.1 \cos(\pi x))$ and $p(x) = 3 + 0.1 \cos(\pi x)$, representing e.g. higher nutrient concentrations and shallower waters near the edge of a lake. The other parameter values are $r = 10$, $h_v = 0.1$, $c = 1$ and $D = 0.01$ (with scaled spatial domain $[-1, 1]$, essentially modelling a lake large enough to allow for coexistence states). As bifurcation parameter we take the spatial average nutrient effect μ . An example bifurcation diagram is given in figure 5(e). This shows the possibility of coexistence states in such systems. In particular, for this specific heterogeneity, the results indicate that a clear lake can tip to a turbid state directly, whereas the transition in the other direction goes via coexistence states in which part of the lake is turbid.

4. Discussion

Classically, tipping in complex systems has been illustrated using simple conceptual models with two alternative states [1–3, 20]. When tipping occurs in these systems, that leads to a reorganization of the full system, with potentially large impacts on its functioning. In this study, we have investigated a prototypical tipping system and extended it by making it spatially explicit, via the incorporation of spatial transport and

spatial heterogeneity. The resulting spatially extended model system revealed a more intricate bifurcation structure with additional branches of stable states compared to the classic ‘S’-curve bifurcation diagram. This is due to the presence of stable coexistence states with part of the spatial domain in one state and part in another. Further, it revealed the possibility of transitions in which the system only undergoes reorganization in part of the spatial domain, limiting the impact of these events on the full system’s functioning. Therefore, this study further specifies how tipping of spatially heterogeneous systems happens; they do not necessarily tip fully in one event, but can have a more fragmented tipping in smaller steps, each corresponding to a restructuring in only part of the spatial domain. These events are therefore less severe than full tipping events, and lead to smaller hysteresis loops. On top of that, while part of the domain is still in its original state, restoration might also be easier and can happen more gradual: as climatic conditions would improve again, the spatial interface between states can move, slowly recovering the system.

This detail of the tipping process might be relevant for many natural systems. Here, we have illustrated this using a few conceptual example systems on different spatial scales, but there are many more. In principle, if a model or real system would allow for bistability locally, spatial effects could lead to the formation of coexistence states—and thus tipping in these systems might be fragmented. One of the prominent examples is the occurrence of multiple convection patterns in ocean general circulation models [66, 67]. Such behaviour was often attributed to numerical artifacts (due to the coarse horizontal resolution in such models). However, the different convection pattern could in the framework here be interpreted as different stable coexistence states. Indeed, the vertical coupling is very strong and follows basically the box model example in section 3.2, whereas the horizontal diffusive coupling is rather weak.

Coexistence states in this study have been characterized by a spatial interface that spatially separates alternative states. Such spatial structures have been observed in reality for systems in which these spatial interfaces are distinct and clearly visible by eye. Examples include the ice grounding line [22] and the tropical forest-savanna boundary [68–70]. In particular, empirical studies of the latter have made connections to the here described mathematical theory [68, 70]. Together with the results on conceptual models presented in this paper, these suggest the relevance of coexistence states for many real climate subsystems. It is difficult to study the associated multistability and resulting fragmented tipping empirically, because of the required temporal and spatial resolution. Nevertheless, at least in more realistic models, the behaviour of e.g. an ice grounding line seems consistent with a fragmented tipping scenario: the interface moves slowly most of the time, with some

sudden events in which interface changes and a larger part of the domain undergoes transition [22]. In addition, there are some early studies suggesting some historic climatic changes, such as atmospheric warming, could be step-like [71], which could be consistent with a fragmented tipping scenario.

As illustrated, the precise importance and relevance of coexistence states depends a lot on the size of the system and the specific heterogeneity. For instance, if a system is too confined, coexistence states cannot form at all, and spatial heterogeneities change the bifurcation structure and the severity of critical transitions. Consequently, for some systems these insights might be more important than for others. Future research should distinguish between climate subsystems that can show fragmented tipping and those that do not. This difference is important to make, as a fragmented tipping scenario indicates an imminent tipping event does not lead to a full system collapse but still leads to similar problems locally in the regions that change state. Of particular interest are the implications on a planetary scale, as it has been hypothesised planetary tipping might happen in the future [17–19]. If tipping on a planetary scale is fragmented its effects might be limited globally—though they can still be harsh locally.

One of the most important tasks remaining is therefore to distinguish between the type and severity of a tipping event before it happens. Current generic early warning signs seem focused mostly on predicting when an imminent system change is going to happen [28, 72, 73], but not on what is happening then. If it is only a reorganization in a minor part of the spatial domain, it is not necessarily worrisome. Further, in spatially-extended systems early warning signs, like critical slowing down, might only be visible in the part of the domain in which change is going to happen, while it might be absent in the global response. Both of these issues might be tackled by inspection of the spatial structure of the destabilizing perturbation [25].

In this paper, we have deliberately used conceptual models that are very basic and relatively simple to showcase the general phenomenon and argue its generality. In more complex and realistic models, including non-gradient systems, coexistence states and fragmented tipping should also be present in general. However, dynamics of such models can be much more difficult. For instance, models with 2D or 3D spatial domains, the spatial interfaces can have complicated structures, and in systems with multiple components might also undergo bifurcations [37, 61, 74, 75].

Finally, we have focused on stationary states, but also the transient behaviour of coexistence states is relevant. When not in equilibrium, a spatial interface slowly moves towards its equilibrium position, hereby converting part of the domain from one state to another—but slowly [36, 37]. This is in contrast

with the tipping events, in which change is fast. Together, this leads to a potentially complicated transient behaviour, which can consist of long periods of slow behaviour interspersed with few fast tipping events [25, 33]. If we would have a better understanding of this transient behaviour of the spatial interface, and how it is influenced by climate change and (human-made) heterogeneities, it might be possible to create circumstances that allow these systems to slowly restore themselves naturally more easily.

Summarising, the take-home messages of this work are as follows. First, the bifurcation structure of any spatially heterogeneous model can be severely more complicated than that of a non-spatial model because of additional branches of coexistence states. Second, the possibility of these coexistence states indicates that tipping in these systems can be fragmented—and thus more gradual—with multiple smaller steps instead of one large tipping event. Third, restoration of a system that has tipped to a coexistence state is easier than from a fully tipped state, because restoration can happen gradually by movement of the spatial interface and because hysteresis loops are smaller. Fourth, the specifications of both the spatial size and the precise spatial heterogeneity determine the precise response of a spatially extended system. This includes to what extent coexistence states and the described fragmented tipping scenario are relevant for the system under consideration. Fifth, examples of many climate subsystems, ranging from global to local scales, suggest coexistence states can emerge on many spatial scales. All this together implies that tipping in many climate (sub)systems might be fragmented and that these systems might be more resilient than indicated by non-spatial models.

Data availability statement

No new data were created or analysed in this study.

Acknowledgments

We thank Valerie Engelmayer for bringing to our attention the coexistence states in stratocumulus clouds. This project is TiPES contribution #137: This project has received funding from the European Union's Horizon 2020 research and innovation programme under Grant Agreement 820970.

Appendix A. Mathematical theory of coexistence states

In this appendix section, we briefly explain the mathematical ideas behind the presented coexistence states. This does not constitute a rigorous mathematical proof; many details, in particular in the spatially heterogeneous case, warrant a further, more careful mathematical investigation.

A.1. Spatially homogeneous equation

Equilibrium solutions to (3) (in one spatial dimension) have to satisfy

$$0 = Dy_{xx} + f(y; \mu), \quad (\text{A.1})$$

where the subscripts x denote taking the derivative with respect to x . This is a Hamiltonian dynamical system (see e.g. [76, chapter 9]) with Hamiltonian H given by

$$H(y, y_x; \mu) = D \frac{y_x^2}{2} + V(y; \mu) \quad (\text{A.2})$$

where V is the potential function, i.e. V satisfies

$$\frac{\partial V}{\partial y}(y; \mu) = f(y; \mu). \quad (\text{A.3})$$

Solutions to (A.1) therefore lie on the level curves with constant $H(y, y_x; \mu)$. Depending on the value of the (bifurcation) parameter μ , the level sets can trace out different orbits in the phase space; see figure A.1.

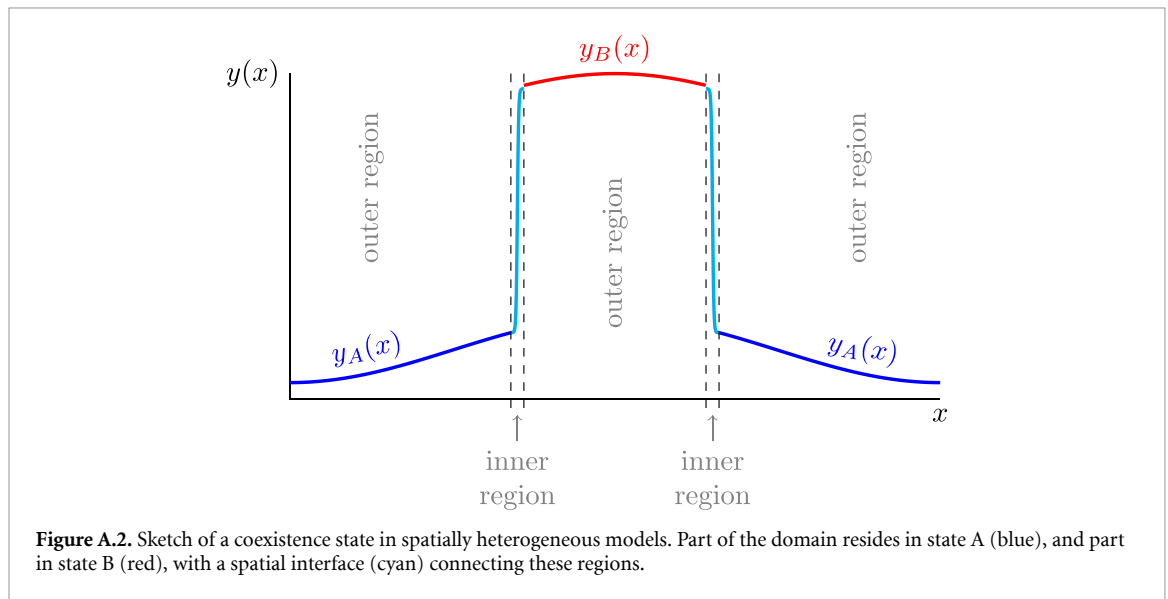
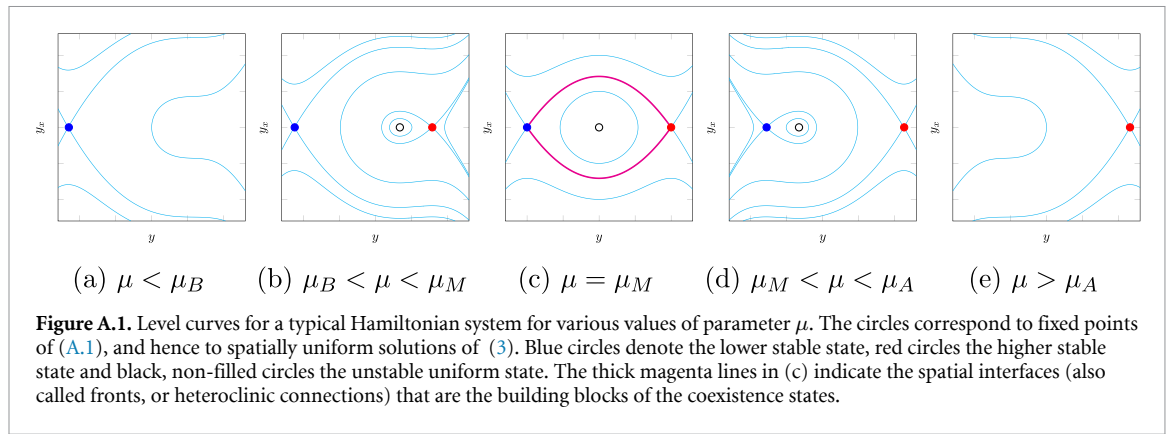
Equilibrium solutions to (A.1) are represented in these phase portraits as bounded orbits. For $\mu < \mu_B$, the only bounded solution is the point $(y, y_x) = (y_A, 0)$ corresponding to the uniform solution $y(x) \equiv y_A$ to (A.1). At $\mu = \mu_B$ a saddle-node bifurcation occurs which creates two other uniform solutions $(y(x) \equiv y_B$ and another, unstable one). For $\mu_B < \mu < \mu_M$, there are additional bounded solutions: a homoclinic orbit connecting $(y_B, 0)$ to itself (corresponding to a pulse solution to (A.1)) and periodic orbits, but these are all unstable solutions to the PDE. At $\mu = \mu_M$, the Maxwell point, the points $(y_A, 0)$ and $(y_B, 0)$ lie on the same level curve, i.e. $\Delta H(\mu) := H(y_A, 0; \mu) - H(y_B, 0; \mu) = V(y_A; \mu) - V(y_B; \mu) = 0$ for $\mu = \mu_M$, and heteroclinic connections between both points exist, which represent the stable equilibrium coexistence states to (3). For $\mu_M < \mu < \mu_A$, there is a homoclinic orbit to $(y_A, 0)$, and periodic orbits that are all unstable. Finally, for $\mu > \mu_A$ only the uniform solution $y(x) \equiv y_B$ exists.

A.2. Spatially heterogeneous equation—existence of equilibrium solutions

Equilibrium solutions to (4) (in one spatial dimension) satisfy

$$0 = Dy_{xx} + f(y, x; \mu). \quad (\text{A.4})$$

We set $D = \varepsilon^2 \ll 1$ (a change of coordinate x can achieve this) and we assume that $\frac{\partial f}{\partial x}(y, x; \mu) \leq \mathcal{O}(1)$ (with respect to ε). In this setting, coexistence solutions to (A.4) have the form as depicted in figure A.2: there are large, so-called outer regions that reside in the same state and small, so-called inner regions in which the transitions between regions are located (i.e. the spatial interfaces). Solutions to (A.4) can now be constructed per region, and should be matched at the boundaries. Here, we only give a sketch of the



leading order construction per region. We note that a rigorous extension of the ideas formulated here would require higher-order terms and matching of the regions. See e.g. [77, chapter 2] for more general explanation on the here employed matched asymptotics method.

In the outer region, (A.4) becomes at leading order the equation

$$0 = f(y, x; \mu), \tag{A.5}$$

with the added constraint that y needs to be smooth. That is, in the outer regions, the diffusion term does not play a role at leading order. Hence, this leads to $y(x) = y_A(x)$ or $y = y_B(x)$.

In the inner regions, we use the coordinate change $\xi := \frac{x-x_F}{\varepsilon}$, where we zoom in on the position $x = x_F$ where the interface is located. We then obtain

$$0 = y_{\xi\xi} + f(y, x_F; \mu) + \varepsilon \frac{\partial f}{\partial x}(y, x_F; \mu)\xi + h.o.t, \tag{A.6}$$

where *h.o.t.* stands for the higher-order terms. At leading order this equation does not depend on space (for any given x_F). Hence, the theory of interfaces in

the spatial homogeneous model applies. That is, by extending the definition of V in (A.3) to

$$\frac{\partial V}{\partial y}(y, x; \mu) = f(y, x; \mu), \tag{A.7}$$

and defining

$$\Delta H(x, \mu) := V(y_A(x), x; \mu) - V(y_B(x), x; \mu), \tag{A.8}$$

it is now clear that an interface can only be located at $x = x_F$ when $\Delta H(x_F, \mu) = 0$.

A.3. Spatially heterogeneous equation—stability of equilibrium solutions

For any given stationary state $y = y^*$, the (linear) stability can be analyzed by setting $y(x, t) = y^*(x) + e^{\lambda t} \bar{y}(x)$ in (4), which yields the linear stability problem

$$\lambda \bar{y} = \varepsilon^2 \bar{y}_{xx} + \frac{\partial f}{\partial y}(y^*, x; \mu) \bar{y}. \tag{A.9}$$

Again, this equation can be analyzed per region.

In the outer regions we have approximately

$$\lambda \bar{y} = \frac{\partial f}{\partial y}(y^*, x; \mu) \bar{y}. \tag{A.10}$$

So an outer region contributes to the spectrum all values $\lambda = \frac{\partial f}{\partial y}(y^*(x), x; \mu)$ for all x within the outer region. Heuristically, this means that the solution becomes unstable in an outer region if the local dynamics (so ignoring all spatial effects) would become unstable.

In the inner regions we have

$$\begin{aligned} \lambda \bar{y} &= \bar{y}_{\xi\xi} + \frac{\partial f}{\partial y}(y^*, x_F; \mu) \bar{y} \\ &+ \varepsilon \frac{\partial^2 f}{\partial x \partial y}(y^*, x_F; \mu) \bar{y}_{\xi} + h.o.t. \end{aligned} \tag{A.11}$$

This equation can be tackled by using a method similar to the one employed in [61, 62]. For this, we first differentiate (A.6) with respect to ξ to obtain

$$0 = y_{\xi\xi\xi}^* + \frac{\partial f}{\partial y}(y^*, x_F; \mu) y_{\xi}^* + \varepsilon \frac{\partial^2 f}{\partial x \partial y}(y^*, x_F; \mu) y_{\xi\xi}^* \tag{A.12}$$

$$+ \varepsilon \frac{\partial f}{\partial x}(y^*, x_F; \mu) + h.o.t. \tag{A.13}$$

Then, by using this equation, it can be seen that substitution of $\bar{y} = y_{\xi}^* + \varepsilon \tilde{y}$ and $\lambda = \varepsilon \tilde{\lambda}$ into (A.11) yields at leading order the equation

$$\tilde{y}_{\xi\xi} + \frac{\partial f}{\partial y}(y^*, x_f; \mu) \tilde{y} = \tilde{\lambda} y_{\xi}^* + \frac{\partial f}{\partial x}(y^*, x_F; \mu). \tag{A.14}$$

A Fredholm solvability condition then indicates that each inner region contributes an eigenvalue

$$\lambda = -C\varepsilon \int_{I_f} \frac{\partial f}{\partial x}(y^*(\xi), x_F; \mu) y_{\xi}^*(\xi) d\xi \tag{A.15}$$

$$= -C\varepsilon \int_{I_f} \frac{d}{d\xi} \left(\frac{\partial V}{\partial x}(y^*(\xi), x_F; \mu) \right) d\xi \tag{A.16}$$

$$= -C\varepsilon \frac{\partial V}{\partial x}(y^*, x_F; \mu)|_{\partial I_f}, \tag{A.17}$$

where $C > 0$ is a constant, and I_f is the inner region.

Thus, λ is proportional to the difference between $\frac{\partial V}{\partial x}$ at both ends of the interface. Or, put differently, to the derivative of ΔH . If the interface under consideration goes from state B to state A , we have $\lambda = -C \frac{\partial \Delta H}{\partial x}(x_F; \mu)$ and if it goes from A to B we have $\lambda = C \frac{\partial \Delta H}{\partial x}(x_F; \mu)$.

The equilibrium solution y^* is only stable if all λ in the spectrum have negative real parts. Therefore, this is only the case when (a) all outer regions are locally stable and (b) all interfaces are located at positions that yield only negative eigenvalues λ .

Appendix B. The small domain limit

If the spatial domain is too small (compared to the diffusion strength), spatial interfaces do not fit in the domain and coexistence states cannot form. If the domain is really small, the spatial heterogeneity becomes irrelevant and dynamics are essentially similar to a model that has no spatial effects. To see this, consider the following spatially heterogeneous model with one spatial dimension (see also e.g. [77, chapter 5] for a more general treatment of so-called homogenization methods):

$$\frac{\partial y}{\partial t} = D \frac{\partial^2 y}{\partial x^2} + f(y, x; \mu) \tag{B.1}$$

on the domain $[-L, L]$ with no-flux boundary conditions. By scaling $x \rightarrow x/L$, we obtain

$$\frac{\partial y}{\partial t} = \frac{D}{L^2} \frac{\partial^2 y}{\partial x^2} + f(y, x; \mu) \tag{B.2}$$

on the domain $[-1, 1]$. Now, in the small domain limit, $\tilde{D} := \frac{D}{L^2} \gg 1$.

Hence, solutions can be approximated using perturbation techniques. Specifically, we can set

$$y(x, t) = y_0(x, t) + \mathcal{O}\left(\frac{1}{\tilde{D}}\right). \tag{B.3}$$

Then, at leading order,

$$\frac{\partial^2 y_0}{\partial x^2} = 0 \tag{B.4}$$

which indicates that $y_0(x, t) \equiv y_0(t)$ is uniform in space.

Then, the evolution of the spatial average $\langle y \rangle(t)$ can be found at leading order:

$$\frac{d}{dt} \langle y \rangle(t) = \frac{1}{2} \int_{-1}^1 \frac{\partial y}{\partial t}(x, t) dx \tag{B.5}$$

$$\begin{aligned} &= \frac{1}{2} \int_{-1}^1 \tilde{D} \frac{\partial^2 y}{\partial x^2}(x, t) dx \\ &+ \frac{1}{2} \int_{-1}^1 f(y, x, \mu) dx \end{aligned} \tag{B.6}$$

$$= \frac{1}{2} \int_{-1}^1 f(y_0, x; \mu) dx + \mathcal{O}\left(\frac{1}{\tilde{D}}\right), \tag{B.7}$$

where the integral over the spatial derivatives vanishes because of the no-flux boundary conditions. Since y_0 is uniform in space, the remaining integral is only the spatial average over the heterogeneity. That is,

$$\frac{d}{dt} \langle y \rangle(t) = f(\langle y \rangle, t) := \frac{1}{2} \int_{-1}^1 f(\langle y \rangle, x; \mu) dx \tag{B.8}$$

which has dynamics similar to a non-spatial model.

Appendix C. Details of the ocean convection model

To model the possibility of bistability between convective and non-convective states, we use a standard box model that models the temperature T and salinity S of the mixed-layer as dynamic variables, which change through the exchange with static atmosphere and ocean boxes [53–56]. We have extended the model by the incorporation of a spatial dimension and the inclusion of spatial diffusion:

$$\frac{\partial T}{\partial t} = D \frac{\partial^2 T}{\partial x^2} + k_T (T_A(x) - T) - \kappa(\Delta\rho) (T - T_0(x)); \quad (C.1)$$

$$\frac{\partial S}{\partial t} = D \frac{\partial^2 S}{\partial x^2} + k_S (S_A(x) - S) - \kappa(\Delta\rho) (S - S_0(x)), \quad (C.2)$$

where $\Delta\rho := \rho - \rho_0$ is the density difference between the mixed-layer and the deep ocean. Further, $T_A(x)$ and $S_A(x)$, respectively $T_0(x)$ and $S_0(x)$, are the space-dependent (reference) temperature and salinity of the atmosphere and deep ocean box, respectively. k_T and k_S give the rate of exchange with the atmosphere box and $\kappa(\Delta\rho)$ the rate of exchange with the deep ocean box. The latter is a function of $\Delta\rho$, which is a non-negative increasing function [53]. That is, convection happens when the exchange rate $\kappa(\Delta\rho)$ is large, which typically occurs if the mixed-layer is heavy enough compared to the deep ocean.

Equations (C.1) and (C.2) describe the evolution of temperature T and salinity S in the ocean's mixed layer. We further simplify this two-component model as follows: density ρ is approximated as a linear equation of state, i.e. $\rho = -\alpha T + \beta S$. Then, T and S are re-scaled as $\tilde{T} = \alpha T$, $\tilde{S} = \beta S$ such that $\rho = \tilde{S} - \tilde{T}$ and the system becomes

$$\frac{\partial \tilde{T}}{\partial t} = D \frac{\partial^2 \tilde{T}}{\partial x^2} + k_T (\tilde{T}_A(x) - \tilde{T}) - \kappa(\Delta\rho) (\tilde{T} - \tilde{T}_0(x)); \quad (C.3)$$

$$\frac{\partial \tilde{S}}{\partial t} = D \frac{\partial^2 \tilde{S}}{\partial x^2} + k_S (\tilde{S}_A(x) - \tilde{S}) - \kappa(\Delta\rho) (\tilde{S} - \tilde{S}_0(x)). \quad (C.4)$$

Now, we assume $k_T = k_S$. Then, we define the spiciness $\mu := \tilde{S} + \tilde{T}$, and $\Delta\rho := \rho - \rho_0 = -(\tilde{T} - \tilde{T}_0) + (\tilde{S} - \tilde{S}_0)$ and $\Delta\mu := \mu - \mu_0 = (\tilde{T} - \tilde{T}_0) + (\tilde{S} - \tilde{S}_0)$. The system can then be rewritten in terms of $\Delta\rho$ and $\Delta\mu$ as

$$\frac{\partial \Delta\rho}{\partial t} = D \frac{\partial^2 \Delta\rho}{\partial x^2} + k_T (\Delta\rho_A(x) - \Delta\rho) - \kappa(\Delta\rho) \Delta\rho + D \frac{\partial^2 \rho_0(x)}{\partial x^2} \quad (C.5)$$

$$\frac{\partial \Delta\mu}{\partial t} = D \frac{\partial^2 \Delta\mu}{\partial x^2} + k_T (\Delta\mu_A(x) - \Delta\mu) - \kappa(\Delta\rho) \Delta\mu + D \frac{\partial^2 \mu_0(x)}{\partial x^2}. \quad (C.6)$$

Since the equation for $\Delta\rho$ does not depend on $\Delta\mu$, it can be solved without taking $\Delta\mu$ into account. Hence, for the purposes here, only the equation for $\Delta\rho$ is needed.

Appendix D. Details of the shallow lake model

The shallow lake model that has been created in [15] is non-spatial and dimensional. It is given by the following ordinary differential equation

$$\frac{dA}{dt} = r \left(\frac{N}{N + h_N} \right) \left(\frac{h_v}{h_v + V(A)} \right) A - cA^2, \quad (D.1)$$

where

$$V(A) = \frac{h_A^p}{h_A^p + A^p}. \quad (D.2)$$

We define $\hat{\mu} := \frac{N}{N + h_N}$ and rescale $\hat{A} = A/h_A$, $\hat{c} = h_A c$ to obtain the scaled model

$$\frac{d\hat{A}}{dt} = r\hat{\mu} \frac{1}{1 + \hat{V}(\hat{A})} \hat{A} - \hat{c}\hat{A}^2, \quad (D.3)$$

where

$$\hat{V}(\hat{A}) = \frac{1}{h_v} \frac{1}{1 + \hat{A}^p}. \quad (D.4)$$

With spatial effects added (and dropping the hats), this becomes the model in (14).

ORCID iDs

Robbin Bastiaansen  <https://orcid.org/0000-0002-5628-8360>

Anna S von der Heydt  <https://orcid.org/0000-0002-5557-3282>

References

- [1] Lenton T M 2013 Environmental tipping points *Annu. Rev. Environ. Resour.* **38** 1–29
- [2] Scheffer M, Carpenter S, Foley J A, Folke C and Walker B 2001 Catastrophic shifts in ecosystems *Nature* **413** 591–6
- [3] Holling C S 1973 Resilience and stability of ecological systems *Annu. Rev. Ecol. Evol. Syst.* **4** 1–23
- [4] Drijfhout S, Bathiany S, Beaulieu C, Brovkin V, Claussen M, Huntingford C, Scheffer M, Sgubin G and Swingedouw D 2015 Catalogue of abrupt shifts in Intergovernmental Panel on Climate Change climate models *Proc. Natl Acad. Sci.* **112** E5777–86
- [5] Lenton T M, Held H, Kriegler E, Hall J W, Lucht W, Rahmstorf S and Schellnhuber H J 2008 Tipping elements in the earth's climate system *Proc. Natl Acad. Sci.* **105** 1786–93
- [6] Hirota M, Holmgren M, Van Nes E H and Scheffer M 2011 Global resilience of tropical forest and savanna to critical transitions *Science* **334** 232–5

- [7] Carla Staver A, Archibald S and Levin S A 2011 The global extent and determinants of savanna and forest as alternative biome states *Science* **334** 230–2
- [8] Rietkerk M and van de Koppel J 1997 Alternate stable states and threshold effects in semi-arid grazing systems *Oikos* **79** 69–76
- [9] Rietkerk M, van den Bosch F and van de Koppel J 1997 Site-specific properties and irreversible vegetation changes in semi-arid grazing systems *Oikos* **80** 241–52
- [10] Stocker T F and Wright D G 1991 Rapid transitions of the ocean's deep circulation induced by changes in surface water fluxes *Nature* **351** 729–32
- [11] Lohmann J and Ditlevsen P D 2021 Risk of tipping the overturning circulation due to increasing rates of ice melt *Proc. Natl Acad. Sci.* **118** e2017989118
- [12] Garbe J, Albrecht T, Levermann A, Donges J F and Winkelmann R 2020 The hysteresis of the Antarctic ice sheet *Nature* **585** 538–44
- [13] Pattyn F and Morlighem M 2020 The uncertain future of the antarctic ice sheet *Science* **367** 1331–5
- [14] Huybrechts P and Jan D W 1999 The dynamic response of the Greenland and Antarctic ice sheets to multiple-century climatic warming *J. Clim.* **12** 2169–88
- [15] Scheffer M, Hosper S H, Meijer M L, Moss B and Jeppesen E 1993 Alternative equilibria in shallow lakes *Trends Ecol. Evol.* **8** 275–9
- [16] Lenton T M and Williams H T P 2013 On the origin of planetary-scale tipping points *Trends Ecol. Evol.* **28** 380–2
- [17] Rockström J *et al* 2009 A safe operating space for humanity *Nature* **461** 472–5
- [18] Steffen W *et al* 2018 Trajectories of the earth system in the anthropocene *Proc. Natl Acad. Sci.* **115** 8252–9
- [19] Barnosky A D *et al* 2012 Approaching a state shift in Earth's biosphere *Nature* **486** 52–58
- [20] May R M 1977 Thresholds and breakpoints in ecosystems with a multiplicity of stable states *Nature* **269** 471–7
- [21] van Nes E H and Scheffer M 2005 Implications of spatial heterogeneity for catastrophic regime shifts in ecosystems *Ecology* **86** 1797–807
- [22] Rosier S H R, Reese R, Donges J F, De Rydt J, Gudmundsson G H and Winkelmann R 2021 The tipping points and early warning indicators for Pine Island Glacier, West Antarctica *Cryosphere* **15** 1501–16
- [23] Valdes P 2011 Built for stability *Nat. Geosci.* **4** 414–6
- [24] Rietkerk M, Bastiaansen R, Banerjee S, van de Koppel J, Baudena M and Doelman A 2021 Evasion of tipping in complex systems through spatial pattern formation *Science* **374** eabj0359
- [25] Bastiaansen R, Doelman A, Eppinga M B and Rietkerk M 2020 The effect of climate change on the resilience of ecosystems with adaptive spatial pattern formation *Ecol. Lett.* **23** 414–29
- [26] Gildor H and Tziperman E 2001 Physical mechanisms behind biogeochemical glacial-interglacial CO₂ variations *Geophys. Res. Lett.* **28** 2421–4
- [27] Alkhuayon H, Ashwin P, Jackson L C, Quinn C and Wood R A 2019 Basin bifurcations, oscillatory instability and rate-induced thresholds for Atlantic meridional overturning circulation in a global oceanic box model *Proc. R. Soc. A* **475** 20190051
- [28] Scheffer M *et al* 2012 Anticipating critical transitions *Science* **338** 344–8
- [29] Scheffer M and Carpenter S R 2003 Catastrophic regime shifts in ecosystems: linking theory to observation *Trends Ecol. Evol.* **18** 648–56
- [30] Micke K 2018 Every pixel of GOES-17 imagery at your fingertips *Bull. Am. Meteorol. Soc.* **99** 2217–9
- [31] Allen S M and Cahn J W 1972 Ground state structures in ordered binary alloys with second neighbor interactions *Acta Metall.* **20** 423–33
- [32] Bray A J 2002 Theory of phase-ordering kinetics *Adv. Phys.* **51** 481–587
- [33] Carr J and Pego R L 1989 Metastable patterns in solutions of $u_t = \varepsilon^2 u_{xx} - f(u)$ *Commun. Pure Appl. Math.* **42** 523–76
- [34] Sandstede B 2002 Stability of travelling waves *Handbook of Dynamical Systems* vol 2 (Amsterdam: Elsevier) pp 983–1055
- [35] Pismen L M 2006 *Patterns and Interfaces in Dissipative Dynamics* (Berlin: Springer-Verlag)
- [36] Zelnik Y R and Meron E 2018 Regime shifts by front dynamics *Ecol. Indic.* **94** 544–52
- [37] Bel G, Hagberg A and Meron E 2012 Gradual regime shifts in spatially extended ecosystems *Theor. Ecol.* **5** 591–604
- [38] Ponedel B C and Knobloch E 2016 Forced snaking: localized structures in the real Ginzburg–Landau equation with spatially periodic parametric forcing *Eur. Phys. J. Spec. Top.* **225** 2549–61
- [39] Ponedel B C and Knobloch E 2018 Gap solitons and forced snaking *Phys. Rev. E* **98** 062215
- [40] Budyko M I 1969 The effect of solar radiation variations on the climate of the earth *Tellus* **21** 611–9
- [41] Sellers W D 1969 A global climatic model based on the energy balance of the earth-atmosphere system *J. Appl. Meteorol.* **8** 392–400
- [42] Ikeda T and Tajika E 1999 A study of the energy balance climate model with CO₂-dependent outgoing radiation: implication for the glaciation during the Cenozoic *Geophys. Res. Lett.* **26** 349–52
- [43] North G R, Cahalan R F and Coakley J A Jr 1981 Energy balance climate models *Rev. Geophys.* **19** 91–121
- [44] Ghil M 1976 Climate stability for a Sellers-type model *J. Atmos. Sci.* **33** 3–20
- [45] Bódai T, Lucarini V, Lunkeit F and Boschi R 2015 Global instability in the Ghil–Sellers model *Clim. Dyn.* **44** 3361–81
- [46] Thorndike A 2012 Multiple equilibria in a minimal climate model *Cold Reg. Sci. Technol.* **76** 3–7
- [47] North G R 1984 The small ice cap instability in diffusive climate models *J. Atmos. Sci.* **41** 3390–5
- [48] North G R 1975 Analytical solution to a simple climate model with diffusive heat transport *J. Atmos. Sci.* **32** 1301–7
- [49] Drazin P G and Griffel D H 1977 On the branching structure of diffusive climatological models *J. Atmos. Sci.* **34** 1696–706
- [50] Caldeira K and Kasting J F 1992 Susceptibility of the early earth to irreversible glaciation caused by carbon dioxide clouds *Nature* **359** 226–8
- [51] Hoffman P F and Schrag D P 2002 The snowball earth hypothesis: testing the limits of global change *Terra Nova* **14** 129–55
- [52] Ashwin P and Anna S 2020 Extreme sensitivity and climate tipping points *J. Stat. Phys.* **179** 1531–52
- [53] Welander P 1982 A simple heat-salt oscillator *Dyn. Atmos. Oceans* **6** 233–42
- [54] Lenderink G and Haarsma R J 1994 Variability and multiple equilibria of the thermohaline circulation associated with deep-water formation *J. Phys. Oceanogr.* **24** 1480–93
- [55] Matthijs den T, Dijkstra H A and Wubs F W 2011 Spurious multiple equilibria introduced by convective adjustment *Ocean Modelling* **38** 126–37
- [56] Vellinga M 1998 Multiple equilibria in ocean models as a side effect of convective adjustment *J. Phys. Oceanogr.* **28** 621–33
- [57] Kaiser A, Faranda D, Krumscheid S, Belušić D and Vercauteren N 2020 Detecting regime transitions of the nocturnal and polar near-surface temperature inversion *J. Atmos. Sci.* **77** 2921–40
- [58] Van de Wiel B J H *et al* 2017 Regime transitions in near-surface temperature inversions: a conceptual model *J. Atmos. Sci.* **74** 1057–73
- [59] Rietkerk M, Dekker S C, De Ruiter P C and van de Koppel J 2004 Self-organized patchiness and catastrophic shifts in ecosystems *Science* **305** 1926–9
- [60] Aleman J C *et al* 2020 Floristic evidence for alternative biome states in tropical Africa *Proc. Natl Acad. Sci.* **117** 28183–90

- [61] Bastiaansen R, Carter P and Doelman A 2019 Stable planar vegetation stripe patterns on sloped terrain in dryland ecosystems *Nonlinearity* **32** 2759
- [62] Bastiaansen R, Chirilus-Bruckner M and Doelman A 2020 Pulse solutions for an extended Klausmeier model with spatially varying coefficients *SIAM J. Appl. Dyn. Syst.* **19** 1–57
- [63] Gandhi P, Werner L, Iams S, Gowda K and Silber M 2018 A topographic mechanism for arcing of dryland vegetation bands *J. R. Soc. Interface* **15** 20180508
- [64] Wuyts B, Champneys A R, Verschueren N and House J I 2019 Tropical tree cover in a heterogeneous environment: a reaction-diffusion model *PLoS One* **14** e0218151
- [65] Carla Staver A and Levin S A 2012 Integrating theoretical climate and fire effects on savanna and forest systems *Am. Nat.* **180** 211–24
- [66] Rahmstorf S 1995 Multiple convection patterns and thermohaline flow in an idealized OGCM *J. Clim.* **8** 3028–39
- [67] Rahmstorf S 1994 Rapid climate transitions in a coupled ocean-atmosphere model *Nature* **372** 82–84
- [68] Staal A, Dekker S C, Xu C and van Nes E H 2016 Bistability, spatial interaction and the distribution of tropical forests and savannas *Ecosystems* **19** 1080–91
- [69] Aleman J C and Carla Staver A 2018 Spatial patterns in the global distributions of savanna and forest *Glob. Ecol. Biogeogr.* **27** 792–803
- [70] Wuyts B, Champneys A R and House J I 2017 Amazonian forest-savanna bistability and human impact *Nat. Commun.* **8** 1–12
- [71] Jones R N and Ricketts J H 2017 Reconciling the signal and noise of atmospheric warming on decadal timescales *Earth Syst. Dyn.* **8** 177–210
- [72] Scheffer M *et al* 2009 Early-warning signals for critical transitions *Nature* **461** 53–59
- [73] Lenton T M 2011 Early warning of climate tipping points *Nat. Clim. Change* **1** 201–9
- [74] Fernandez-Oto C, Tzuk O and Meron E 2019 Front instabilities can reverse desertification *Phys. Rev. Lett.* **122** 048101
- [75] Jaibi O, Doelman A, Chirilus-Bruckner M and Meron E 2020 The existence of localized vegetation patterns in a systematically reduced model for dryland vegetation *Physica D* **412** 132637
- [76] Meiss J D 2007 *Differential Dynamical Systems* (Philadelphia, PA: SIAM)
- [77] Holmes M H 2012 *Introduction to Perturbation Methods* vol 20 (New York: Springer)